

Konrad-Zuse-Zentrum
für Informationstechnik Berlin

Takustraße 7
D-14195 Berlin-Dahlem
Germany

M. SEEBASS, R. BECK, J. GELLERMANN, J. NADOBNY, P. WUST

**Electromagnetic phased arrays for regional
hyperthermia – optimal frequency and
antenna arrangement**

Electromagnetic phased arrays for regional hyperthermia – optimal frequency and antenna arrangement

M. Seebass^{1*}, R. Beck^{1*}, J. Gellermann², J. Nadobny^{1,2}, P. Wust²

¹Konrad-Zuse-Zentrum für Informationstechnik Berlin
Takustr. 7, 14195 Berlin-Dahlem, Federal Republic of Germany
e-mail: {seebass,beck,nadobny}@zib.de

²Universitätsklinikum Charité, Campus Virchow-Klinikum
Poliklinik und Strahlenklinik
Augustenburger Platz 1, 13344 Berlin-Wedding, Federal Republic of Germany
e-mail: {johanna.gellermann,peter.wust}@charite.de

Abstract. In this paper we investigate the effects of the three-dimensional arrangement of antennas and frequency on temperature distributions that can be achieved in regional hyperthermia using an electromagnetic phased array. We compare the results of power-based and temperature-based optimization. Thus we are able to explain the discrepancies between previous studies favouring more antenna rings on the one hand and more antennas per ring on the other hand. We analyze the sensitivity of the results with respect to changes in amplitudes and phases as well as patient position. This analysis can be used for different purposes. First, it provides additional criteria for selecting the optimal frequency. Second, it can be used for specifying the required phase and amplitude accuracy for a real phased array system. Furthermore, it may serve as a basis for technological developments in order to reduce both types of sensitivities described above.

Key words: Pelvic heating, phased array optimization, electromagnetic hyperthermia, sensitivity analysis

*The work of these authors was supported by Deutsche Forschungsgemeinschaft, Sonderforschungsbereich 273, Germany.

1 Introduction

Regional hyperthermia, i.e. the heating of a larger part of the body, is a treatment method which is primarily applied to deep-seated tumors in the pelvis. Normally, electromagnetic phased arrays are used for this purpose. They consist of several antennas surrounding the patient and emitting radio-waves. Single antennas or groups of antennas are fed by separate power generators. By proper selection of amplitudes and phases of the feeding voltages the interference patterns of the antenna fields can be steered in order to create a therapeutically favourable temperature distribution in the body.

The most common phased array system is the Sigma-60 applicator of BSD Medical Systems, Salt Lake City, Utah. In clinical practice it was found out that there are certain locations of tumors which cannot be heated satisfactorily with this system. Therefore several studies based on numerical simulation have been carried out in order to support the development of improved systems.

Most of these investigations were focusing on configuration parameters like the number and the geometric arrangement of the antennas as well as the frequency of the electromagnetic waves. It turned out that the choice of an appropriate objective function for evaluating the ‘therapeutic quality’ of a certain arrangement is an important issue. In general, objective functions are either based on the distribution of the electromagnetic power deposited in tissue or on the temperature distribution within the patient’s body.

In an earlier simulation study [Wust *et al.* 1996] showed that a *3D control* of the interference pattern can be achieved if the antennas are arranged in two or three rings instead of one. A considerable improvement compared to the Sigma 60 configuration could be shown for a system with three rings, each comprising four antenna pairs. Only a small additional improvement was achieved if the number of antennas per ring was increased further. The results were mainly based on temperature optimization; a frequency of 90 MHz was assumed throughout.

Partly in view of these results, the Sigma-Eye applicator was developed by BSD Medical Systems and introduced in 1996. This applicator contains three rings of four antenna pairs.

In [Paulsen *et al.* 1999] power-based objective functions were used. The effect of frequency was investigated for the first time, as well as a large variety of antenna configurations (one, two, and four rings, between 2 and 24 antennas per ring). One major result was that increasing the number of antennas per ring is in many cases more favourable than increasing the number of antenna rings. Furthermore, frequencies of 150 and 200 MHz yielded better results compared to 100 MHz which was until then considered to be the optimal frequency for regional hyperthermia.

In this paper we once again raise the issues of optimal antenna configuration

and optimal frequency, based on numerical simulations for various patient models. We extend the work of [Paulsen *et al.* 1999] by some investigations relevant for clinical practice:

- Both power-based and temperature-based optimizations are performed. The comparison of the results can explain the discrepancies between [Wust *et al.* 1996] and [Paulsen *et al.* 1999] concerning the effects of increased number of antenna rings vs. increased number of antennas per ring.
- A *sensitivity analysis* is performed in order to obtain an estimate of possible deviations between simulation and clinical practice. Sensitivities with respect to changes in amplitudes and phases as well as patient position are considered. This analysis will provide an additional criterion for selecting the optimal frequency. Beyond that, it may specify the required phase and amplitude accuracy for a real phased array system, and serve as a basis for technological developments that could reduce both types of sensitivities.
- A more realistic geometric shape of the antennas (similar to those of the Sigma-Eye applicator) is assumed, and coupling between the antennas is taken into account.

Reservations have been raised against temperature-based optimization because of the poor knowledge about blood perfusion. However, we point out that for the purpose of comparing different applicator configurations it is not necessary to predict the precise temperature in an individual patient, and some standard values for blood perfusion can be assumed. On the other hand, power-based optimization (ratio of power in the tumor vs. power in healthy tissue) can result in severe hot spots in healthy tissue. Thus [Das *et al.* 1999b] make some suggestions for power-based objective functions which should suppress hot spots. Taking all this into account, our assessment of applicator configurations will mainly be based on temperature optimization. But we emphasize that care has to be taken in using a temperature-based objective function for an individual patient's treatment planning.

2 Methods

The type of simulations performed in this study is essentially the same as in treatment planning. We use the planning system *HyperPlan* which was developed at the Konrad-Zuse-Zentrum Berlin within the framework of the Sonderforschungsbereich 273 'Hyperthermie: Methodik, Klinik und Biologie'. In the following we give a short sketch of the planning procedure.

2.1 Steps of treatment planning

Generation of a patient model. For the numerical calculation of electric fields and temperature distributions *tetrahedral patient models* are used. The generation of a patient model from a set of CT-scans consists of five steps:

First, a manual *segmentation* of the CT data is performed, i.e., the relevant tissue compartments are manually defined on each scan [Stalling *et al.* 1998]. Second, the compartment surfaces are extracted. For this purpose the well-known marching cubes algorithm [Lorensen and Cline 1987] has been generalized for non-binary classifications [Hege *et al.* 1997]. Thereby a consistent description of the compartment interfaces is created. These are composed of so-called patches, each patch separating two different compartments. The resulting surface models typically comprise 200 000 - 500 000 faces. The number of faces must be reduced in order to create models suitable for simulations. A simplification algorithm from computer graphics [Garland and Heckbert 1997] has been adapted for this purpose, specifically avoiding intersections and assuring a high quality (i.e. small aspect ratio) of the surface triangles. Fourth, a volumetric tetrahedral mesh is created for each tissue compartment using an *advancing front* algorithm. Tetrahedron generation starts at the compartment's surface which is composed of the corresponding patches. Repeatedly a triangle of the advancing front is selected and a fourth point is searched such that the resulting tetrahedron resembles an equilateral one as much as possible. This procedure is continued until the whole compartment is filled. Finally the mesh quality is improved by flipping interior edges and faces and shifting interior vertices.

Field calculation. For electromagnetic field simulation an *extended grid* is needed. It includes essential parts of the hyperthermia applicator like the water bolus and the antennas, as well as part of the surroundings, which is assumed to be air. The extended grid has a spherical outer boundary.

The field calculation employs the *Finite Element* (FE) method, where edge elements are used as basis functions for the electric field. The resulting large linear equation systems are solved iteratively by multigrid algorithms. A special hybrid smoothing technique, which utilizes a Helmholtz decomposition of the fields, is implemented for coping with the null-space of the curl-operator. Without this measure, iterative solvers may render a poor convergence behaviour [Beck *et al.* 1999]. Three types of boundary conditions occur in the simulations. The *metallic parts* of the antennas are assumed to be ideal conductors, represented by a homogeneous Dirichlet condition for the tangential component of the electric field. At the *antenna junctions*, an inhomogeneous Cauchy condition is applied. For the incoming wave of an active antenna the electric field is defined at the junction. For the out-

going wave at active and passive antennas the ratio of the tangential components of electric and magnetic field is prescribed, corresponding to the impedance of the feeding line. At the *spherical outer boundary* a first order radiation boundary condition is applied.

The electric fields are calculated separately for each independent channel of the hyperthermia applicator. Then the electric field for an arbitrary choice of amplitudes and phases can be determined by superposition.

Temperature calculation. As a model of heat transport, the *bio-heat transfer equation* (BHTE) is assumed. A solution of the stationary BHTE is computed using the *Finite Element* method. Because the stationary temperature distribution depends linearly on the power deposition pattern, a (slightly more complicated) superposition principle is valid for the BHTE as well. Simulating an applicator with n independent channels, $n^2 + 1$ solutions of the BHTE have to be calculated in advance. Then the temperature distribution for an arbitrary choice of amplitudes and phases can be determined by superposition, for details see [Nikita *et al.* 1993, Das *et al.* 1999a]. This fact is exploited by the temperature optimization algorithm (see below).

Power optimization. The objective function for power optimization corresponds to Method I as defined in [Paulsen *et al.* 1999]. For this objective function [Kremer and Louis 1990] have shown that

- the optimization problem is equivalent to searching for a maximum of P_T/P_H , with P_T and P_H denoting the powers absorbed in tumor and healthy tissue, respectively. This power ratio is except for a constant factor identical with the gain as defined in equation (6) of [Paulsen *et al.* 1999].
- the optimum can be found as follows. If amplitude and phase for antenna i are combined to a complex amplitude z_i , and all complex amplitudes are combined to a complex vector Z , the powers mentioned above can be represented by

$$P_T = Z^* A_T Z \tag{1}$$

$$P_H = Z^* A_H Z \tag{2}$$

with Z^* the transposed, complex conjugate of vector Z , and A_T, A_H hermitian, positive (semi)definite matrices. If we consider the generalized eigenvalue problem

$$A_T Z = \lambda A_H Z , \quad (3)$$

the optimal control is given by the eigenvector corresponding to the largest eigenvalue.

Temperature-based optimization. The objective function for temperature optimization is the same as, e.g., in [Wust *et al.* 1996, Das *et al.* 1999a]:

$$q = \int_{\substack{x \in \text{tumor} \\ T(x) < T_{ther}}} (T_{ther} - T(x))^2 dx + \int_{\substack{x \notin \text{tumor} \\ T(x) > T_{health}}} (T(x) - T_{health})^2 dx \quad (4)$$

This objective function corresponds to the requirements that the temperature in the tumor should be above a therapeutic level T_{ther} , and the temperature in healthy tissue should not exceed a level T_{health} . We use $T_{ther} = 43^\circ\text{C}$ and $T_{health} = 42^\circ\text{C}$. The square root of q can be interpreted as the mean deviation between the actual and the ‘ideal’ temperature distribution, thus we define $1/\sqrt{q}$ as a gain factor which can be compared with the gain factor of power optimization.

In addition the temperature in healthy tissue is constrained by certain limits which depend on the tissue type. Similar to [Nikita *et al.* 1993], the constraints are taken into account via a penalty term. During optimization, the objective function can be calculated very efficiently from the pre-calculated solutions of the BHTE. The same holds for the first and second partial derivatives of the objective function with respect to the antenna parameters, which can be computed without numerical differentiation. For details see [Lang *et al.* 1999].

Sensitivity analysis. This analysis is only performed for the results of temperature optimization. Sensitivity with respect to *amplitudes and phases* is evaluated by some kind of Monte-Carlo method. The amplitudes and phases are assumed to be randomly distributed in a given interval around the optimal values. For 1000 samples of antenna parameter settings, the corresponding temperature distributions are determined, again by applying the superposition of pre-calculated solutions. For each sample the so-called T_{90} -value (the temperature level exceeded in 90% of the tumor volume) is computed. The sensitivity of an optimal control is measured by the difference between T_{90} at the optimum and the median of the distribution of T_{90} -values. The median value is taken because the distributions show a distinct asymmetry (see figure 3).

Sensitivity with respect to *patient positioning* is determined by moving the patient model by a certain distance (in both directions) along each of the coordinate axes. This analysis is much more expensive than the former one, because a new

FE simulation of electric field and temperature distribution must be performed for each of the six patient positions. Again the T_{90} -temperatures are calculated, and the difference between the optimal and the minimal value is taken as a measure of sensitivity.

2.2 Design of the study.

Selection of patient models. Five of the hyperthermia patients from Charité Medical Center at Berlin were selected. Their tumor types and tumor locations are considered to be representative for regional hyperthermia.

- Patient 1: proximally and presacrally located rectum carcinoma
- Patient 2: distally located rectum carcinoma
- Patient 3: cervical carcinoma
- Patient 4: prostate carcinoma
- Patient 5: peripherally located soft tissue sarcoma

The tetrahedral patient models consist of 80 000 - 150 000 tetrahedra. The mean and maximal edge lengths are 1.6 and 3.0 cm, respectively. Figure 1 shows cross-sections of the patient models indicating the tumor locations.

Applicator and dipole antennas. For this study an applicator with *elliptical cross-section* is assumed. The long and short axes are 55 and 45 cm, respectively. These dimensions correspond to a ‘mean applicator’ between the Sigma-60 and the Sigma-Eye. The applicator length is 50 cm.

Electric dipole antennas are positioned at the elliptical applicator surface. Their dimensions correspond to the Sigma-Eye applicator: total length 12.7 cm, distance at the junction 0.65 cm, width at the junction 0.65 cm, width at the tip 1.3 cm. As mentioned above, the boundary conditions at the antenna junctions allow for outgoing waves. In this way coupling between antennas is taken into account. The impedance of the feeding lines is assumed to be 50 Ohm.

Antenna configurations and frequencies. The antenna configurations are characterized by the number of antenna rings and the number of antennas per ring. For practical reasons the number of rings is not increased above three. An analysis of the Sigma-Eye applicator [Wust *et al.* 2000] has shown that the electrically short dipole antennas require special impedance matching networks, and there is substantial longitudinal coupling between the antenna rings. Both effects would

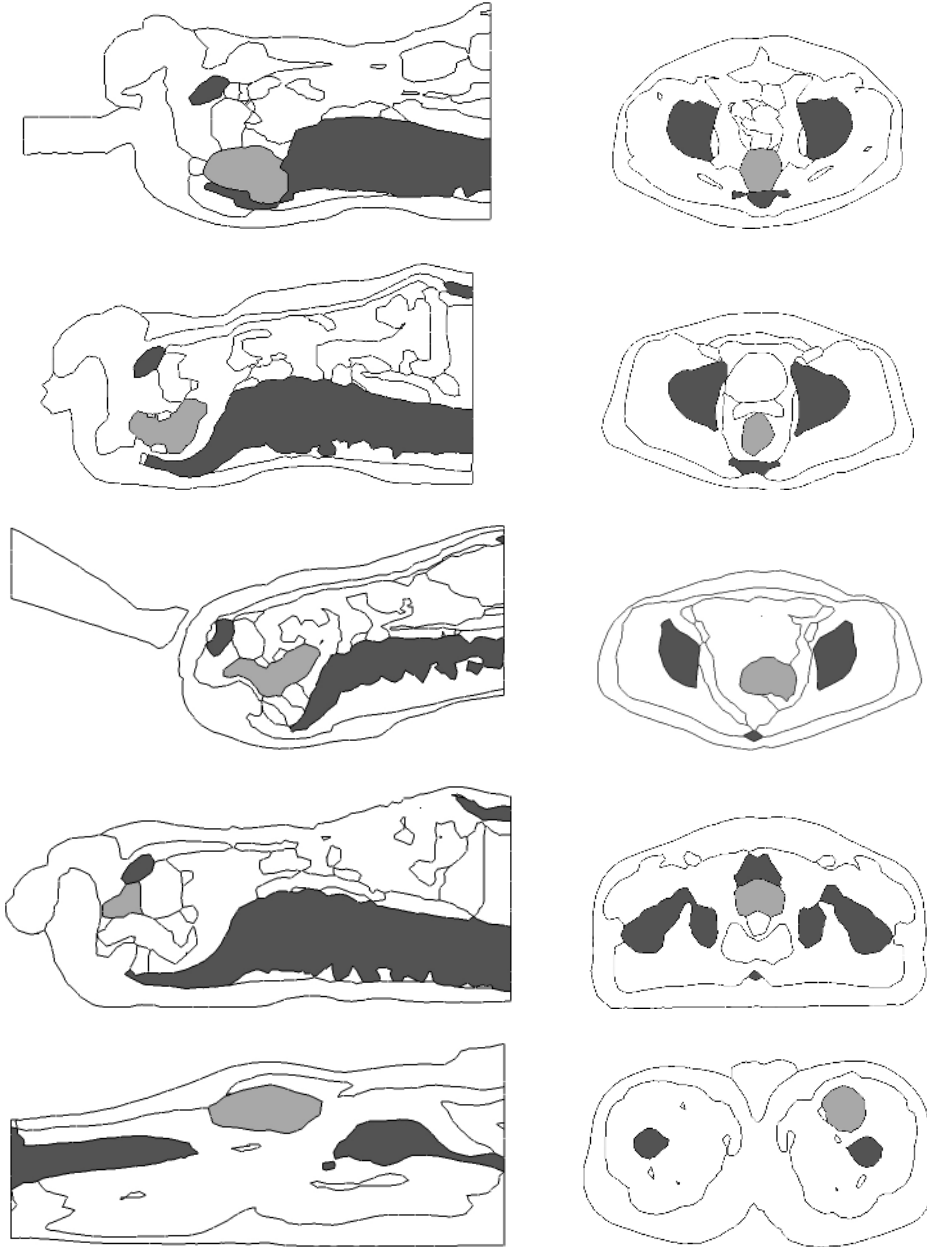


Figure 1: Sagittal and transversal cross-sections of five patient models.
Light grey: tumor, dark grey: bone.

be even more pronounced for a larger number of rings. The longitudinal distances of the antenna junctions are 17.7 cm and 15.2 cm for two and three antenna rings, respectively.

Either 8 or 12 antennas are positioned equidistantly on the elliptical surface of each ring. The following configurations are studied: 4 antenna pairs, 6 antenna pairs, 8 single antennas, and 12 single antennas per ring. Antenna pairs are investigated because (1) thereby applicators very similar to the Sigma-60 and Sigma-Eye are included in the study, (2) the pairs create a more uniform power distribution than four or six single antennas, and (3) the number of (time-consuming) field calculations can be reduced.

Similar to [Paulsen *et al.* 1999], excitation frequencies of 100, 150, and 200 MHz are taken into account. The CPU times for the field calculations depend heavily on the frequency. Typical CPU times for computations of one antenna field are 40, 50, and 80 minutes on an SGI Onyx2 workstation (MIPS 10 000 processor, 195 MHz) for 100, 150, and 200 MHz, respectively. Altogether, $3 * 4 * 3 = 36$ different ‘applicator types’ are compared for each patient model.

Electric and thermal tissue properties. The electric tissue properties assumed in the simulations are shown in table 1. For most tissue types the data agree with [Paulsen *et al.* 1999]. For vessels, lung, and spleen the data are taken from [Gabriel *et al.* 1996]. Tumor tissue is assumed to have the same electric properties as muscle.

Tissue type	100 MHz		150 MHz		200 MHz	
	ϵ_r	σ	ϵ_r	σ	ϵ_r	σ
Fat	9.4	0.052	9.1	0.054	8.8	0.055
Muscle	66.0	0.71	63.1	0.725	60.2	0.74
Bone	15.0	0.06	14.45	0.067	13.9	0.074
Vessels	76.8	1.23	71.25	1.26	68.5	1.28
Lung	31.6	0.306	28.3	0.322	26.6	0.335
Kidney	98.0	0.81	88.0	0.873	78.0	0.935
Liver	69.0	0.487	63.4	0.5225	57.8	0.558
Spleen	90.7	0.802	78.8	0.858	72.7	0.901
Intestine	60.32	0.63	57.3	0.668	53.68	0.7
Bladder	58.0	1.21	55.1	1.28	51.62	1.34
Tumor	66.0	0.71	63.1	0.725	60.2	0.74
Water Bolus	78.0	0.0	78.0	0.0	78.0	0.0
Background (Air)	1.0	0.0	1.0	0.0	1.0	0.0

Table 1: Electric tissue properties: relative dielectric constant ϵ_r and electric conductivity σ [$1 / (\Omega * m)$].

The thermal tissue properties are summarized in table 2. For healthy tissues also the temperature limits T_{lim} for optimization are listed. They are set to 42°C for sensitive organs like bladder, kidney, liver etc., 43°C for intestine, and 44°C otherwise. For tissue perfusion elevated values are assumed which occur as a response to heating. Only the largest vessels are represented in the patient models. For them a ‘very large’ perfusion value is prescribed, which essentially keeps the vessels at arterial blood temperature (37°C). This has a significant influence on tumor temperature for the patients 3 and 5, where large vessels are in direct neighbourhood of the tumor.

Tissue type	κ [W/(m * K)]	ρ [kg/m ³]	W [ml/(100g * min)]	T_{lim} [°C]
Fat	0.21	900	5	44.0
Muscle	0.642	1000	20	44.0
Bone	0.436	1600	5	44.0
Vessels	0.506	1000	500	44.0
Lung	0.2	500	20	42.0
Kidney	0.577	1000	400	42.0
Liver	0.64	1000	100	42.0
Spleen	0.577	1000	60	42.0
Intestine	0.55	1000	20	43.0
Bladder	0.6	1000	30	42.0
Tumor	0.642	1000	5	-

Table 2: Thermal tissue properties: thermal conductivity κ , density ρ , perfusion W , and temperature limits for optimization T_{lim} .

Parameters for sensitivity analysis. For the analysis of sensitivity with respect to amplitudes and phases the accuracy of power amplitudes is assumed to be 10% of the maximal value and the phase accuracy is assumed to be 5°. These limits refer to the values at the antenna junctions. Even a higher accuracy of the generator output is required in order to warrant this precision.

Sensitivity with respect to patient positioning is analyzed by moving the patient model by ± 1 cm in x-, y-, and z-direction. Because this analysis is quite expensive, it has been only performed for the three-ring configurations. In radiation therapy, the positioning accuracy is generally better than 1 cm. However, in regional hyperthermia the situation is less satisfactory, e.g. due to the water bolus and the different shapes of the table of the CT scanner and the ‘hammock’ of the hyperthermia applicator; thus an accuracy of 1 cm in position seems to be an ambitious goal. An improved accuracy may be expected from a hyperthermia system integrated in a magnetic resonance tomograph, which allows for a control of patient positioning by MR scans.

3 Results

Table 3 shows the results of power optimization. Similar to [Paulsen *et al.* 1999], the gain factors P_T/P_H were normalized to the result for the Sigma-60 configuration (one ring, four antenna pairs, 100 MHz). For each frequency and number of rings a linear regression was performed. It describes the normalized gain factors of all patients as a function of the number of channels per ring. The number of channels is identical with the number of pairs for the four- and six-pair configurations, and with the number of antennas for the eight- and twelve-antenna configurations. The results are visualized in figure 2, top row. For most of the regression lines we have found a large variation of data between the five patients. However, general trends can be identified. For the one-ring configurations the gain factors are only weakly influenced by the frequency. For the two-ring configurations they exhibit a maximum at 150 MHz. For the three-ring configurations there is a large increase from 100 to 150 MHz and only a marginal further increase at 200 MHz.

Table 4 shows the results of temperature optimization. They are visualized in figure 2, bottom row. As before, the gain factors $1/\sqrt{q}$ (with q as defined in equation 4) were normalized to the Sigma-60 configuration. For the one- and two-ring configurations the gain factor shows a small increase with the frequency, whereas in the case of the three-ring configurations the gain factor increases significantly with the frequency. As can be seen in table 4, patients 3 and 5 do not obey this rule; here the gain factor for the three-ring configurations depends only weakly on the frequency.

The sensitivity with respect to amplitudes and phases (table 5) increases with the number of channels per ring and decreases with the frequency. Figure 3 shows as an example the histogram of T_{90} -values for patient 5 with 3 x 12 antennas at 150 MHz. For the majority (85%) of configurations the sensitivity is at an acceptable level below 0.2°C . However, some configurations show a high sensitivity above 1.0°C . For these cases the contributions of amplitude and phase errors were analyzed separately. It was found that the main contribution ($> 90\%$) is due to amplitude errors.

Table 6 shows the sensitivities with respect to patient positioning for the three-ring configurations. The sensitivity exhibits no systematic dependence on the number of channels per ring, but increases (with a few exceptions) steeply with the frequency. In most cases patient movements up and down in the y-direction (anterior - posterior) cause the largest deviations from the optimal temperature distribution. For patient 5 there is also a high sensitivity for movements in x-direction (left-right). In more than 60% of the cases the sensitivity is larger than 1.0°C .

Patient 1 (proximal and presacral rectum carcinoma)									
# of rings ant. / ring	100 MHz			150 MHz			200 MHz		
	1	2	3	1	2	3	1	2	3
4p	1.0	0.93	1.1	0.90	1.4	1.7	1.4	1.3	1.8
6p	1.1	1.1	1.1	0.92	1.6	1.9	1.3	1.1	1.5
8	1.2	1.2	1.4	1.1	1.8	2.2	1.5	1.5	2.0
12	1.3	1.4	1.7	1.5	2.2	2.6	2.1	1.9	2.9
Patient 2 (distal rectum carcinoma)									
# of rings ant. / ring	100 MHz			150 MHz			200 MHz		
	1	2	3	1	2	3	1	2	3
4p	1.0	1.0	1.2	0.88	1.3	1.7	1.3	1.6	2.2
6p	1.1	1.3	1.4	0.90	1.6	2.0	1.2	1.3	1.9
8	1.2	1.4	1.5	0.90	1.4	1.9	1.4	1.7	2.4
12	1.3	1.5	1.7	1.3	2.1	2.6	1.7	1.7	2.7
Patient 3 (cervical carcinoma)									
# of rings ant. / ring	100 MHz			150 MHz			200 MHz		
	1	2	3	1	2	3	1	2	3
4p	1.0	1.1	1.2	0.82	1.3	1.6	0.86	0.97	1.7
6p	1.1	1.2	1.3	0.77	1.4	1.7	0.98	1.0	1.9
8	1.1	1.3	1.4	0.86	1.5	1.8	1.1	1.1	2.1
12	1.2	1.4	1.5	1.1	1.6	2.0	1.2	1.3	2.2
Patient 4 (prostate carcinoma)									
# of rings ant. / ring	100 MHz			150 MHz			200 MHz		
	1	2	3	1	2	3	1	2	3
4p	1.0	0.98	1.2	0.86	1.1	1.5	1.0	0.94	1.6
6p	1.1	1.1	1.3	0.86	1.2	1.8	0.92	0.95	1.5
8	1.1	1.1	1.3	0.88	1.1	1.6	1.0	1.0	1.7
12	1.2	1.2	1.4	0.96	1.4	2.0	1.1	1.1	1.8
Patient 5 (soft tissue sarcoma)									
# of rings ant. / ring	100 MHz			150 MHz			200 MHz		
	1	2	3	1	2	3	1	2	3
4p	1.0	1.0	1.1	0.72	0.84	1.2	0.66	0.99	1.2
6p	1.5	1.6	1.9	1.2	1.7	2.3	1.2	1.6	1.9
8	1.7	1.8	2.1	1.3	1.7	2.4	1.4	1.9	2.6
12	1.9	2.1	2.4	1.7	2.6	3.4	2.0	2.4	3.2

Table 3: Gain factors of power optimization (normalized to the Sigma-60-configuration with one ring and four antenna pairs at 100 MHz).

Patient 1 (proximal and presacral rectum carcinoma)									
# of rings ant. / ring	100 MHz			150 MHz			200 MHz		
	1	2	3	1	2	3	1	2	3
4p	1.0	1.5	1.6	0.94	1.7	2.7	1.3	1.8	2.7
6p	1.0	1.7	1.9	1.0	1.7	2.8	1.5	2.0	3.0
8	1.0	1.7	1.9	0.98	1.8	3.2	1.5	2.5	3.6
12	1.0	1.8	2.0	1.1	2.0	3.4	1.6	2.7	4.3
Patient 2 (distal rectum carcinoma)									
# of rings ant. / ring	100 MHz			150 MHz			200 MHz		
	1	2	3	1	2	3	1	2	3
4p	1.0	1.4	1.6	0.96	1.4	2.4	1.4	2.0	3.6
6p	1.0	1.6	1.8	1.0	1.5	2.7	1.3	1.8	3.7
8	1.0	1.6	1.8	1.0	1.5	2.8	1.6	2.6	4.4
12	1.1	1.6	1.9	1.1	1.8	3.1	1.7	2.3	5.3
Patient 3 (cervical carcinoma)									
# of rings ant. / ring	100 MHz			150 MHz			200 MHz		
	1	2	3	1	2	3	1	2	3
4p	1.0	1.6	1.7	0.79	1.4	1.7	1.1	0.91	1.7
6p	1.0	1.7	1.8	0.82	1.5	1.8	1.1	1.3	1.7
8	1.2	1.7	1.8	1.0	1.5	1.9	1.2	1.1	1.8
12	1.2	1.8	1.9	1.2	1.6	1.9	1.4	1.5	1.9
Patient 4 (prostate carcinoma)									
# of rings ant. / ring	100 MHz			150 MHz			200 MHz		
	1	2	3	1	2	3	1	2	3
4p	1.0	1.2	1.4	1.0	1.4	1.8	1.1	1.2	1.7
6p	1.0	1.3	1.7	1.0	1.5	2.0	1.1	1.4	2.1
8	1.0	1.5	1.8	1.1	1.4	2.0	1.1	1.4	2.2
12	1.0	1.5	1.9	1.1	1.6	2.2	1.1	1.6	2.6
Patient 5 (soft tissue sarcoma)									
# of rings ant. / ring	100 MHz			150 MHz			200 MHz		
	1	2	3	1	2	3	1	2	3
4p	1.0	1.2	1.4	0.68	0.80	1.1	0.71	0.97	1.2
6p	1.1	1.3	1.4	1.0	1.4	1.5	1.0	1.3	1.5
8	1.1	1.3	1.4	1.1	1.5	1.6	1.1	1.4	1.6
12	1.2	1.4	1.5	1.1	1.5	1.6	1.2	1.5	1.7

Table 4: Gain factors of temperature optimization (normalized to the Sigma-60-configuration with one ring and four antenna pairs at 100 MHz).

Patient 1 (proximal and presacral rectum carcinoma)									
# of rings ant. / ring	100 MHz			150 MHz			200 MHz		
	1	2	3	1	2	3	1	2	3
4p	0.11	0.21	0.15	0.12	0.14	0.03	0.06	0.08	0.01
6p	0.11	0.12	0.05	0.12	0.13	0.07	0.08	0.03	0.05
8	0.12	0.14	0.06	0.10	0.16	0.02	0.10	0.11	0.04
12	0.16	0.13	0.37	0.16	0.51	0.05	0.07	0.02	0.02
Patient 2 (distal rectum carcinoma)									
# of rings ant. / ring	100 MHz			150 MHz			200 MHz		
	1	2	3	1	2	3	1	2	3
4p	0.03	0.04	0.05	0.05	0.05	0.06	0.05	0.02	0.05
6p	0.03	0.02	0.18	0.06	0.03	0.02	0.13	0.00	0.01
8	0.03	0.00	0.12	0.02	0.07	0.05	0.01	0.12	0.00
12	0.14	0.20	0.39	0.07	0.35	0.11	0.03	0.07	0.00
Patient 3 (cervical carcinoma)									
# of rings ant. / ring	100 MHz			150 MHz			200 MHz		
	1	2	3	1	2	3	1	2	3
4p	0.06	0.14	0.08	0.05	0.13	0.07	0.06	0.07	0.07
6p	0.07	0.13	0.11	0.06	0.14	0.10	0.07	0.13	0.17
8	0.12	0.18	0.08	0.05	0.14	0.13	0.07	0.22	0.11
12	0.62	1.70	3.23	0.18	1.20	0.46	0.07	0.16	0.38
Patient 4 (prostate carcinoma)									
# of rings ant. / ring	100 MHz			150 MHz			200 MHz		
	1	2	3	1	2	3	1	2	3
4p	0.01	0.09	0.11	0.04	0.06	0.07	0.01	0.01	0.05
6p	0.01	0.10	0.10	0.02	0.05	0.05	0.01	0.01	0.01
8	0.02	0.02	0.11	0.04	0.05	0.04	0.01	0.01	0.02
12	0.03	0.22	1.00	0.06	0.12	0.11	0.00	0.00	0.02
Patient 5 (soft tissue sarcoma)									
# of rings ant. / ring	100 MHz			150 MHz			200 MHz		
	1	2	3	1	2	3	1	2	3
4p	0.02	0.08	0.69	0.04	0.08	0.43	0.11	0.13	0.24
6p	0.01	0.34	0.65	0.01	0.04	0.06	0.02	0.07	0.00
8	0.05	0.38	1.61	0.03	0.26	0.06	0.04	0.33	0.06
12	1.96	3.51	3.54	0.02	1.40	0.41	0.03	0.38	0.13

Table 5: Sensitivity with regard to amplitude and phase variations ($\pm 10\%$ of maximum power, $\pm 5^\circ$). Differences in T_{90} -temperatures [$^\circ\text{C}$] between optimal control and median from 1000 samples.

Patient 1 (presacral rectum carcinoma)						
ant. / ring	100 MHz		150 MHz		200 MHz	
4p	0.51	z	0.54	y	2.41	y
6p	0.72	z	1.41	y	1.77	y
8	0.42	z	0.95	y	1.84	y
12	0.45	y	1.42	y	2.17	y
Patient 2 (distal rectum carcinoma)						
ant. / ring	100 MHz		150 MHz		200 MHz	
4p	0.28	z	1.51	y	2.93	y
6p	0.45	y	1.42	y	2.72	y
8	0.54	y	1.43	y	3.06	y
12	0.32	y	1.50	y	2.75	y
Patient 3 (cervical carcinoma)						
ant. / ring	100 MHz		150 MHz		200 MHz	
4p	0.61	y	1.57	y	1.92	y
6p	0.70	y	1.01	y	1.08	y
8	1.00	z	1.49	y	1.32	y
12	1.56	z	1.12	y	1.21	y
Patient 4 (prostate carcinoma)						
ant. / ring	100 MHz		150 MHz		200 MHz	
4p	0.30	y	0.78	y	1.24	y
6p	0.31	z	0.64	y	1.07	y
8	1.09	x	0.73	y	1.93	y
12	0.78	z	0.75	y	2.31	y
Patient 5 (soft tissue sarcoma)						
ant. / ring	100 MHz		150 MHz		200 MHz	
4p	1.07	x	0.90	x	2.06	y
6p	1.47	y	1.55	x	1.80	x
8	0.83	y	1.33	y	1.86	x
12	2.70	y	1.00	x	1.86	x

Table 6: Sensitivity with regard to positioning for three-ring configurations. Difference in T_{90} -temperatures [°C] between optimal control and minimum of six samples (± 1 cm) and direction of movement for which the minimum occurred.

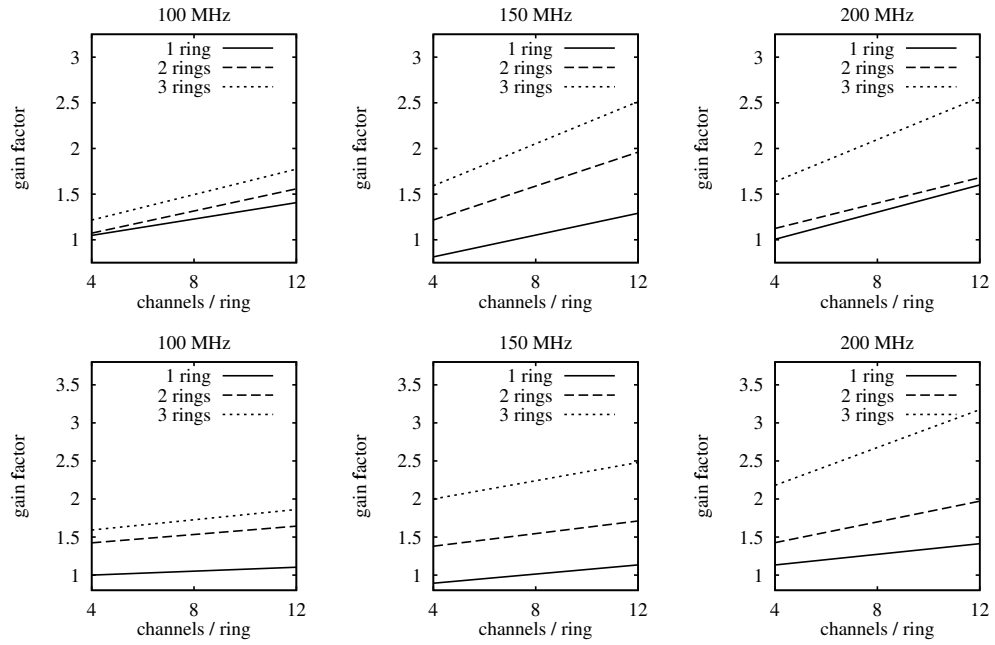


Figure 2: Results of power optimization (top row) and temperature optimization (bottom row). Linear regression of the normalized gain factor as a function of the number of channels per ring; mean of five patient models.

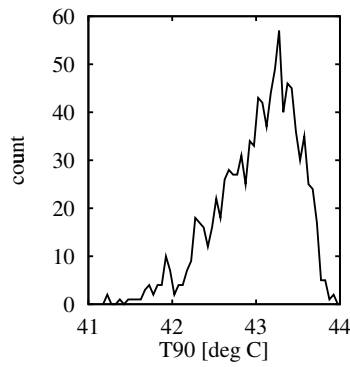


Figure 3: Analysis of sensitivity with respect to amplitudes and phases. Histogram of T_{90} -values from 1000 samples for patient 5 with 3 x 12 antennas at 150 MHz.

4 Discussion

Comparison with the previous study. The results of power optimization agree qualitatively with [Paulsen *et al.* 1999], which, e.g., can be seen on comparison of patients 2 and 3 of this study (centrally located tumors) with site 8 of the previous study. Note that the configurations chosen for normalization slightly differ: one ring, eight antennas in [Paulsen *et al.* 1999], one ring, four antenna pairs in this study. Generally the four and six antenna pairs considered here perform slightly better than the four or six single antennas used in the previous study.

Power and temperature optimization The comparison of the top and bottom row in figure 2 shows that the number of channels per ring on general has a bigger effect in power optimization, where especially for the one-ring configurations the increase of the gain factor with the number of channels is significantly higher. For temperature optimization the number of rings plays a more important role, and the two- and three-ring configurations generally create larger gain factors than the one-ring configurations. As an example, consider the different twelve-channel configurations in tables 3 and 4: one ring, twelve antennas (1 x 12), two rings, six antenna pairs (2 x 6p), and three rings, four antenna pairs (3 x 4p). For power optimization, in 8 of 15 cases the 1 x 12 configuration achieves the highest gain factor. On the other hand, for temperature optimization, in 12 of 15 cases the 3 x 4p configuration shows the best performance.

Our explanation for the differences between power and temperature optimization is as follows: power optimization primarily exploits a *constructive* interference of the antenna fields within the tumor. This interference is likely to be maximal if a large number of antennas is arranged in one plane around the tumor, i.e. one ring. On the other hand, a main goal in temperature optimization is the suppression of hot spots in healthy tissue by *destructive* interference of the antenna fields. The hot spots typically occur at different locations within the patient's body, especially with respect to the z-direction. A *3D-control* is needed for an effective hot spot suppression, and thus the two- or three-ring configurations are more favourable for temperature optimization.

For patient 5 no significant hot spots occur far away from the tumor due to its location in the upper thigh. Thus for temperature optimization the influence of the number of antenna rings is smaller for this patient.

Sensitivity. We do not have a conclusive explanation for the facts that the largest sensitivities with respect to amplitudes and phases occur at low frequencies, and that they are dominantly caused by amplitude errors. The optimal settings for these configurations show a significant pattern: all but a few antennas adjacent

to one another have very low power levels; for these antennas the phases differ by nearly 180° , so that the ‘dominant modes’ of the antenna fields cancel each other. These adjustments appear to be particularly sensitive.

Conversely, the sensitivity with respect to patient positioning steeply increases with the frequency. We suppose that this is caused by resonance effects which can be seen in the water bolus. For high frequencies the distance between the patient’s body and the elliptical bolus boundary is larger than half a wavelength, thus an excitation of eigenmodes may occur, which is strongly influenced by movements of the patient.

Optimal antenna configuration and frequency. This assessment is based on the results of temperature optimization, cf. table 4. For an effective hot spot reduction two or three antenna rings are needed. At 150 and 200 MHz the best results are clearly achieved with three antenna rings. The number of channels per ring plays a less important role, but its influence increases with frequency. The optimal frequency for the three-ring configurations lies between 150 and 200 MHz; it slightly increases with the number of channels. For patients 3 and 5 the results for the three-ring configurations depend only weakly on frequency. This may be due to the fact, that – at least for patient 5 – hot spot reduction is not as important as for the other patients.

The sensitivities shown in tables 5 and 6 suggest that a large number of channels per ring and high frequencies should be avoided. The best compromise seem to be three antenna rings, six or eight channels per ring, and a frequency around 150 MHz.

5 Conclusion

Based on numerical simulations the effects of different parameters of an electromagnetic phased array for regional hyperthermia were studied. These parameters include the antenna arrangement (number of antenna rings and number of antennas per ring) as well as the excitation frequency. Both power-based and temperature-based optimizations were carried out. Comparison of the respective results showed significant differences favouring more antennas per ring on the one hand and more antenna rings on the other hand. Thus the discrepancies between previous studies could be explained.

A sensitivity analysis was introduced in this study for the first time. It provides an estimate how far a real treatment may deviate from the simulated optimum, and can be considered a valuable supplement to the optimization.

For an effective hot spot reduction, which is an important issue in clinical

practice, three-ring antenna configurations proved to be optimal. Taking into account the results of sensitivity analysis, optimal values of the other parameters are six or eight channels per ring and a frequency around 150 MHz.

Future work may have its focus on the following topics:

- In this study configurations including four or six antenna pairs per ring have been investigated for a number of reasons (see section 2.2). The modeling of the antenna pairs is to some extent idealized in assuming identical incoming waves for both antennas of each pair. A recent analysis of the Sigma-Eye applicator [Wust *et al.* 2000], which compared simulations and field measurements, has shown that considerable deviations from this assumption can occur, and it would be difficult to model the real applicator including its sophisticated feeding network. With this background it seems questionable if antenna pairs should be used at all. Six single antennas per ring should be investigated as an alternative to six antenna pairs per ring considered here.
- The sensitivity analysis initiated in this study raises new questions. The mechanisms behind the increase or decrease of sensitivity with frequency, as well as its dependence on other parameters, are not quite clear. A better understanding may provide the basis for devising less sensitive systems, thus achieving a more reliable correspondence between simulation and real treatment. For example, if the sensitivity with respect to patient positioning can be shown to be caused by resonance effects, one could try to reduce it by inserting absorbing structures into the water bolus.

For a less sensitive system the optimal applicator parameters may shift towards an increased number of channels per ring and a higher frequency.

- The sensitivity with respect to other inaccuracies should be studied, e.g., uncertainties of the electric and thermal tissue properties. The analysis of patient movements could be extended to rotations and elastic deformations.

Acknowledgement. The authors are indebted to P. Deuffhard and H.-C. Hege from Konrad-Zuse-Zentrum at Berlin for their continuing support of this project. We thank H. Ganter from Charité Medical Center at Berlin for performing the manual segmentation of the CT data.

References

- [Beck *et al.* 1999] Beck, R., Deuffhard, P., Hiptmair, R., Hoppe, R. H. W., and Wohlmuth, B. (1999). Adaptive multilevel methods for edge element discretizations of Maxwell's equations. *Surv. Math. Ind.*, 8:271–312.
- [Das *et al.* 1999a] Das, S. K., Clegg, S. T., and Samulski, T. V. (1999a). Computational techniques for fast hyperthermia temperature optimization. *Med. Phys.*, 26:319–328.
- [Das *et al.* 1999b] Das, S. K., Clegg, S. T., and Samulski, T. V. (1999b). Electromagnetic thermal therapy power optimization for multiple source applicators. *Int. J. Hyperthermia*, 15:291–308.
- [Gabriel *et al.* 1996] Gabriel, S., Lau, R. W., and Gabriel, C. (1996). The dielectric properties of biological tissues III. Parametric models for the dielectric spectrum of tissues. *Phys. Med. Biol.*, 41:2271–2293.
- [Garland and Heckbert 1997] Garland, M. and Heckbert, P. S. (1997). Surface simplification using quadric error metrics. In *Computer Graphics (Proc. SIGGRAPH '97)*, pages 209–216.
- [Hege *et al.* 1997] Hege, H.-C., Seebass, M., Stalling, D., and Zöckler, M. (1997). A generalized marching cubes algorithm based on non-binary classifications. Technical report, SC 97-05, Konrad-Zuse-Zentrum für Informationstechnik Berlin, Takustr. 7, D-14195 Berlin, Germany.
- [Kremer and Louis 1990] Kremer, J. and Louis, A. K. (1990). On the mathematical foundations of hyperthermia therapy. *Math. Meth. Appl. Sci.*, 13:467–479.
- [Lang *et al.* 1999] Lang, J., Erdmann, B., and Seebass, M. (1999). Impact of nonlinear heat transfer on temperature control in regional hyperthermia. *IEEE Trans. Biomed. Eng.*, 46:1129–1138.
- [Lorensen and Cline 1987] Lorensen, W.E. and Cline, H.E. (1987). Marching cubes: a high resolution 3d surface construction algorithm. *Computer Graphics*, 21:163–169.
- [Nikita *et al.* 1993] Nikita, K. S., Maratos, N. G., and Uzunoglu, N. K. (1993). Optimal steady-state temperature distribution for a phased array hyperthermia system. *IEEE Trans. Biomed. Eng.*, 40:1299–1306.

- [Paulsen *et al.* 1999] Paulsen, K. D., Geimer, S., Tang, J., and Boyse, W. E. (1999). Optimization of pelvic heating rate distributions with electromagnetic phased arrays. *Int. J. Hyperthermia*, 15:157–186.
- [Stalling *et al.* 1998] Stalling, D., Zöckler, M., and Hege, H.-C. (1998). Segmentation of 3D medical images with subvoxel accuracy. In Lemke, H. U., Inamura, K., Vannier, M. W., and Farman, A. G., editors, *Computer Assisted Radiology and Surgery (Proc. CAR'98)*, pages 137–142.
- [Wust *et al.* 1996] Wust, P., Seebass, M., Nadobny, J., Deuffhard, P., Mönich, G., and Felix, R. (1996). Simulation studies promote technological development of radiofrequency hyperthermia. *Int. J. Hyperthermia*, 12:477–494.
- [Wust *et al.* 2000] Wust, P., Beck, R., Berger, J., Föhling, H., Seebass, M., Włodarczyk, W., Hoffmann, W., and Nadobny, J. (2000). Electric field distributions in a phased-array applicator with 12 channels - measurements and numerical simulations. *Med. Phys.*, 27, in press.